The Journal of Immunology

Accelerated Antigen Sampling and Transport by Airway Mucosal Dendritic Cells following Inhalation of a Bacterial Stimulus

Frode L. Jahnsen, Deborah H. Strickland, Jennifer A. Thomas, Iriani T. Tobagus, Sylvia Napoli, Graeme R. Zosky, Debra J. Turner, Peter D. Sly, Philip A. Stumbles and Patrick G. Holt

J Immunol 2006; 177:5861-5867; ;
doi: 10.4049/jimmunol.177.9.5861
http://www.jimmunol.org/content/177/9/5861

The Journal of Immunology is published twice each month by
The American Association of Immunologists, Inc.,
1451 Rockville Pike, Suite 650, Rockville, MD 20852

Print ISSN: 0022-1767 Online ISSN: 1550-6606.

Accelerated Antigen Sampling and Transport by Airway Mucosal Dendritic Cells following Inhalation of a Bacterial Stimulus[1]

Frode L. Jahnsen,[2]*† Deborah H. Strickland,[2]* Jennifer A. Thomas,* Iriani T. Tobagus,* Sylvia Napoli,* Graeme R. Zosky,* Debra J. Turner,* Peter D. Sly,* Philip A. Stumbles,* and Patrick G. Holt[3]*

An increase in the tempo of local dendritic cell (DC)-mediated immune surveillance is a recognized feature of the response to acute inflammation at airway mucosal surfaces, and transient up-regulation of the APC functions of these DC preceding their emigration to regional lymph nodes has recently been identified as an important trigger for T cell-mediated airway tissue damage in diseases such as asthma. In this study, using a rat model, we demonstrate that the kinetics of the airway mucosal DC (AMDC) response to challenge with heat-killed bacteria is considerably more rapid and as a consequence more effectively compartmentalized than that in recall responses to soluble Ag. Notably, Ag-bearing AMDC expressing full APC activity reach regional lymph nodes within 30 min of cessation of microbial exposure, and in contrast to recall responses to nonpathogenic Ags, there is no evidence of local expression of APC activity within the airway mucosa preceding DC emigration. We additionally demonstrate that, analogous to that reported in the gut, a subset of airway intraepithelial DC extend their processes into the airway lumen. This function is constitutively expressed within the AMDC population, providing a mechanism for continuous immune surveillance of the airway luminal surface in the absence of "danger" signals. ***The Journal of Immunology,*** **2006, 177: 5861–5867.**

The main function of the mucosal immune system is surveillance for Ags associated with viruses and bacteria. This defense mechanism includes both innate and adaptive components, with the role of the innate arm being a combination of acute attack on the pathogens and rapid transmission of relevant alarm signals to the adaptive immune system (1). The rate-limiting step in the latter role involves the sampling of microbial material by resident mucosal dendritic cells (DC),[4] their migration to regional lymph nodes (RLN), and their subsequent activation of rare Ag-specific naive T cells. The precise mechanisms underlying these DC functions in vivo are poorly understood, and in particular there are no studies that have approached definition of the maximum kinetics of this process under conditions of natural challenge of the airway mucosa.

In comparison to intermittent exposure to live microbes, the respiratory mucosal immune system is exposed much more frequently to microbial (especially bacterial) breakdown products, which are ubiquitous in normal indoor environments and the have the potential to trigger the same range of surveillance mechanisms. Moreover these products have recently been recognized as powerful modifiers of immune responses to nonmicrobial Ags in inspired air, including aeroallergens associated with diseases such as atopic asthma. The potential effects of these agents in this context range from subversion of local mucosal tolerance mechanisms to promote allergen specific Th cell sensitization (2) to deviation of ensuing responses toward a nonpathogenic Th1-like phenotype (3), but the mechanisms by which exposure to these agents influences local Ag sampling mechanisms remains poorly understood.

In the current study we have sought to more precisely characterize the resident DC populations in the central airways, focusing in particular on the nature of the acute changes in their distribution, migration pattern, and APC activity induced by exposure to a locally applied bacterial stimulus.

Materials and Methods

Animals and aerosol exposure

Inbred PVG rats were bred and maintained free of pathogens at the Telethon Institute for Child Health Research. Animals of both sexes age 8–12 wk were used. They were exposed for 60 min to an aerosol by Tri-R Airborne Infection Apparatus (model A4-2X; Tri-R Instruments) of OVA prepared at 1% in PBS stock solutions and stored at 4°C (Sigma-Aldrich) or exposed to heat-killed *Moraxella catarrhalis* organisms (hospital isolate) suspended in PBS at 10^9 CFU/ml either alone or coadministered together with aerosolized OVA. OVA sensitization of animals was achieved by i.p. injection of 500 μl of an OVA (200 μg/ml)/alum suspension, given 14 days before use in challenge experiments. The Telethon Institute for Child Health Research Animal Experimentation Ethics Committee, operating under guidelines set by the National Health and Medical Research Council of Australia, approved all animal experimentation protocols.

Media and reagents

Tissue culture medium was RPMI 1640 with glutamine (Invitrogen Life Technologies), supplemented with 20 μg/ml gentamicin, 20 μM 2-ME, and 5% FCS or 1% normal rat serum (NRS) (RPMI-5% FCS or RPMI-1%

*Telethon Institute for Child Health Research, Centre for Child Health Research, University of Western Australia, West Perth, Australia; and †Laboratory of Immunohistochemistry and Immunopathology, Institute of Pathology, University of Oslo and The Pathology Clinic Rikshospitalet-Radiumhospitalet Medical Center, Oslo, Norway

Received for publication March 17, 2006. Accepted for publication August 10, 2006.

The costs of publication of this article were defrayed in part by the payment of page charges. This article must therefore be hereby marked *advertisement* in accordance with 18 U.S.C. Section 1734 solely to indicate this fact.

[1] This work was supported by the National Health and Medical Research Council of Australia.

[2] F.L.J. and D.H.S. are joint first authors.

[3] Address correspondence and reprint requests to Professor Patrick G. Holt, Division of Cell Biology, Telethon Institute for Child Health Research, P.O. Box 855, West Perth WA 6872, Australia. E-mail address: patrick@ichr.uwa.edu.au

[4] Abbreviations used in this paper: DC, dendritic cell; AMDC, airway mucosal DC; IEDC, intraepithelial DC; LN, lymph node; RLN, regional LN; NRS, normal rat serum; FSC, forward light scatter; SSC, side light scatter.

0022-1767/06/$02.00

NRS, respectively). For isolation of cells, type IV collagenase (1.5 mg/ml; Worthington) and pancreatic type I DNase (0.1 mg/ml; Sigma-Aldrich) were used in GKN buffer (11 mM D-glucose, 5.5 mM KCl, 137 mM NaCl, 25 mM Na_2HPO_4, and 5.5 mM $NaH_2PO_4 2H_2O$) supplemented with 10% FCS (GKN-10% FCS) for enzymatic digestion of tissues or GKN with 5% FCS (GKN-5% FCS) for other steps. All mAbs (BD Pharmingen) and immunostaining reagents used for flow cytometry have been previously described (4, 5). Immunophenotypic analysis was performed using a four-color FACSCalibur (BD Biosciences) and FlowJo software (Tree Star). FITC and tetramethylrhodamine isothiocyanate (TRITC) powder were purchased from Sigma-Aldrich and FITC-conjugated dextran from Molecular Probes.

Cell preparation and culture

Single cell suspensions of RLN, parathymic lymph nodes (LN), and superficial cervical LN and tracheal digests were prepared using standard methods and depleted of macrophages and B cells as previously described (4). In brief, LN were collected after rats were killed by CO_2 asphyxiation. They were sliced with a scalpel and then digested with type IV collagenase and type I DNase in GKN-10% FCS at 37°C for 30 min in a shaking water bath. For collection of main conducting airways (trachea), rats were euthanized by an i.p. injection of 3 ml of phenobarbitone sodium (Lethabarb; Virbac) during halothane anesthesia. Trachea was excised, flushed with PBS, opened longitudinally, cut finely transversely, and finally cut randomly. Tissue was transferred into GKN-10% FCS containing type IV collagenase (1.5 mg/ml) and type I DNase and incubated for 90 min at 37°C in a shaking water bath. After 60 min, additional type I DNase was added to the digestion mixture. Following completion of digestion, tissue was disrupted with a plastic transfer pipette. The digest mixture was then passed through a cotton wool filter to remove tissue debris followed by centrifugation at 1800 rpm for 7 min. The pellet was resuspended in GKN-5% FCS and any RBC or remaining tissue debris was removed using a Lymphoprep gradient (density 1.077 g/ml; Axis-Shield), and centrifuged at 1500 rpm for 15 min. The cells at the interface were collected and washed in GKN-5% FCS (1800 rpm for 7 min). The cells (referred to as total tracheal digest cells) were then diverted to various other procedures as required. For DC isolation/sorting, macrophages were removed by adherence to plastic (45 min at 37°C) in GKN-5% FCS. B cells were removed by depletion using mouse anti-rat κ chain (Ox12; BD Pharmingen) followed by anti-mouse Ig Dynabeads (Dynal Biotech). After B cell and macrophage removal, DC were isolated by immunostaining the remaining cells with FITC-conjugated anti-rat MHC class II (Ox6 FITC; BD Pharmingen), which were then sorted using a Beckman Coulter EPICS Elite ESP, routinely to >94%. Contaminating cells were mainly $CD3^+$ T cells or cytokeratin-positive cells, both <3%.

To distinguish between intraepithelial and subepithelial populations, the tracheas were opened and sliced along the long axis of the tube into equal segments. The tissue was then incubated for 20 min in the digestion mixture followed by scraping with a scalpel to remove the epithelial layer. The denuded lamina propria tissue and the removed epithelium were then minced finely and reincubated for an additional 20 min to release trapped cells.

Coculture experiments using isolated tissue DC from challenged rats and an OVA-responsive T cell line were performed as described (4). In brief, rats were immunized with 200 μl of an emulsion of OVA (1 mg/ml) in CFA (1/1 (Difco) and injected s.c. at the base of tail, 100 μl each side). RLN were collected day 9 postimmunization and cultured (2×10^6/ml) in RPMI-1%NRS and OVA (50 μg/ml) for 5 days. Viable cells were then collected using a Lymphoprep density gradient (as described) and cultured at a density of 2×10^5/ml in RPMI-5%FCS plus 50 U/ml rIL-2. Following expansion in rIL-2, on day 8 cells were restimulated with irradiated thymocyte feeders (10^6/ml) in RPMI-1% NRS plus OVA (50 μg/ml). On day 11, viable cells were harvested from a Lymphoprep gradient and cultured in RPMI-5% FCS plus rIL-2 (50 U/ml) for an additional 3 days. Stocks of OVA T cell line (4×10^7 cells/vial day 7 postrestimulation) were frozen in 10% DMSO in FCS and stored in liquid nitrogen. For OVA-specific T cell proliferation assays, OVA T cell lines were thawed 3 days earlier and cultured in RPMI-5%FCS plus rIL-2. On the day of use, OVA T cell lines were prepared by centrifugation over a Lymphoprep gradient followed by washing three times in RPMI-5% FCS. Cells were cultured at 1×10^5/ml in RPMI-5% FCS plus DC (isolated from various tissues following various treatments at densities as indicated) for 48 h, then pulsed with [^{3}H]thymidine for an additional 18 h. Cell proliferation was determined as the mean cpm from triplicate cultures. All proliferation assays performed used the same frozen stocks of OVA T cell line allowing for direct comparison.

In situ analysis of DC populations

Confocal microscopy studies using whole mount preparations were performed as recently described (4). Fixed specimens were immunostained with mAb Ox6 anti-rat MHC class II combined with rabbit antiserum to rat laminin or cytokeratin, followed by Cy3-labeled goat anti-mouse IgG in combination with Oregon green-labeled goat anti-rabbit IgG (Molecular Probes). The stained samples were washed and mounted in custom-made slides and images obtained with a confocal laser scanning microscope. For cell counts, preparations were optically sectioned at 1-μm increments from the surface epithelial side at a magnification of ×600. At least eight random fields were examined and over 100 intraepithelial, and 200 lamina propria $Ox6^+$ cells were counted per specimen. Identical series of image stacks obtained for each wavelength were then merged, and three-dimensional information (*xyz*-axis) was analyzed with Object Image 2.08 software (an extended version of NIH Image). Staining of frozen sections was performed as described previously (4).

Tracking studies

The technique used to track airway mucosal DC (AMDC) migration to RLN has been previously described (4). In brief, rats were anesthetized and 100 μl of FITC-dextran (10 mg/ml) or 100 μl of FITC (10 mg/ml in PBS) was administered immediately below the vocal cords, or 100 μl of TRITC (5 mg/ml in PBS) was simultaneously injected peritoneally, or vice versa. RLN were removed 24 h later and either snap frozen for immunostaining experiments or enzymatically digested as described.

Methacholine hyperresponsiveness

The techniques used were as previously described (4). Briefly, respiratory impedance (Zrs) was measured by forced oscillation between 0.5 and 20 Hz using a computer-controlled piston ventilator (Flexivent; Scireq). The constant-phase model was fitted to give estimates of airway (Raw) and tissue mechanics (data not shown). Following baseline lung function, methacholine challenge was performed by delivering aerosols (2 min) of saline (control) and methacholine (0.1, 0.3, 1.0, 3.0, 10.0, and 30.0 mg/ml) during tidal ventilation. Five measurements of impedance were made after each dose, and peak responses reported.

Statistics

The experiments were conducted using single animals (tissue sections) or pooled tissue from 10 or more animals and were repeated two to five times as indicated. Unless indicated, unpaired Student's *t* test was performed. Data are shown as the mean ± SE or SD as indicated.

Results

In situ distribution and functional phenotype of steady-state AMDC

First we examined the in situ distribution and the functional phenotypes of AMDC in experimental rats under steady-state conditions. Earlier studies from our and other laboratories have defined populations of DC staining heavily for MHC class II and negative for T and B cell lineage markers and markers expressed on tissue macrophages, both within and below the airway epithelium (4, 6, 7), but focusing principally on the intraepithelial DC (IEDC) population, which can be readily quantified in conventional frozen sections. In this model we applied a new technique in which immunostained whole mount preparations of tracheal tissue were prepared for confocal microscopy that allowed three-dimensional examination of virtually all DC through the full thickness of the trachea. By this method we confirmed our previous findings (4, 6) demonstrating that MHC class II^+ DC constituted a dense network in the resting epithelium (~650 cells/mm^2 surface area, $n = 5$ rats) (Fig. 1*A*). However, these IEDC accounted for only 20 ± 2% of the total AMDC population, whereas the majority (80 ± 2%) were subepithelial (Fig. 1*B*). Compared with their IEDC counterparts, lamina propria DC were often rounder, smaller cells with few dendrites (Fig. 1*B*). These in situ findings were reflected by the forward light scatter (FSC), side light scatter (SSC), and MHC class II surface expression profiles of AMDC prepared by digesting whole trachea (Fig. 1, *C–F*). A median of 78% of the overall AMDC population as defined by R1 (Fig. 1, *D* and *F*, R2+R3

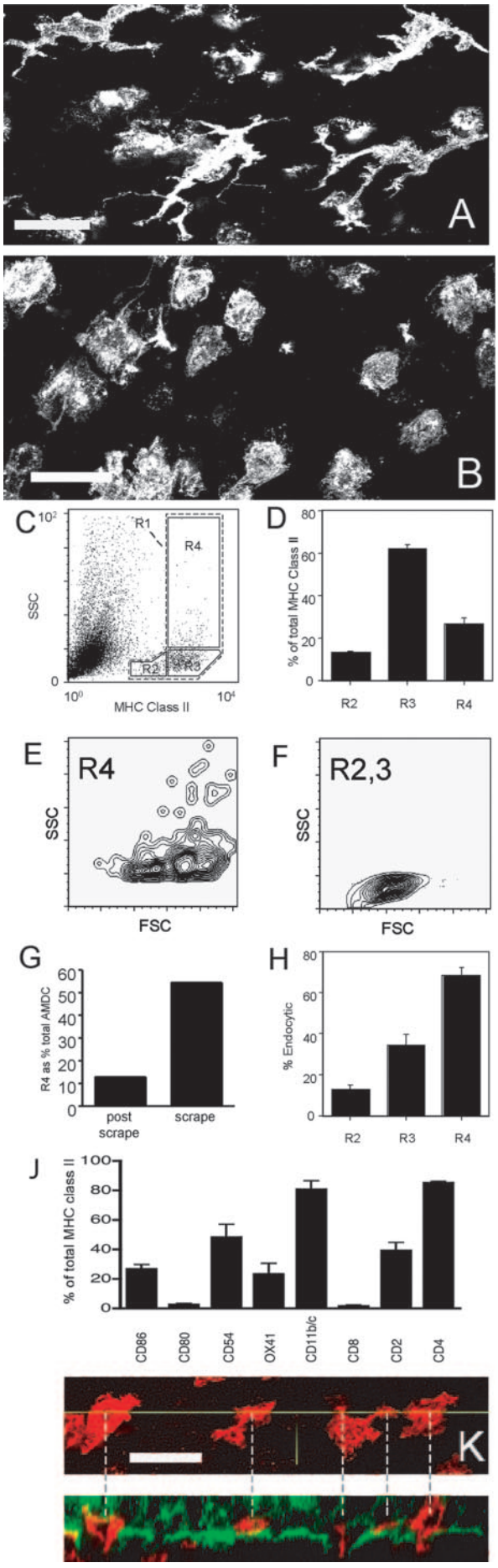

gate) showed lower SSC and FSC, closely resembling the characteristics of smaller lamina propria DC (Fig. 1*B*), whereas the less frequent R4 cells (22% of the overall DC population (Fig. 1*D*) displayed higher SSC and FSC (Fig. 1*E*), consistent with the physical properties of the IEDC (Fig. 1*A*). In a further attempt to distinguish between intraepithelial and subepithelial populations, the epithelial layer was removed from the underlying lamina propria and the cells from the two compartments were digested separately. In accordance with our in situ data, flow cytometric analysis of resulting DC populations showed that the majority (~55%) of the IEDC were MHC class $II^{high}SSC^{high}$ with FSC profiles indicative of large cells (Fig. 1*G*), whereas only a minority of lamina propria DC expressed this phenotype (10–15%) (Fig. 1*G*).

The FSC, SSC, and MHC class II characteristics of AMDC subregions R2–R4 suggested progression through different stages of maturation. To further examine this possibility the endocytic capacity of DC within the three subregions was measured. As determined by dextran-FITC uptake, their endocytic capacity was directly associated with SSC and MHC class II expression. The R4 subregion cells displayed 2- and 4-fold higher activity than R3 and R2 subregion cells, respectively (Fig. 1*H*). Further immunostaining revealed only minor differences in functional surface marker expression between cells in subregions R2, R3, and R4. Of note, the costimulatory molecules CD80 and CD86 were only expressed on a minor population of cells within all three subregions (R4 phenotypic characteristics) as shown in Fig. 1*J*. The similarity in immunophenotype between the DC in these three subregions suggested that they represent a maturational continuum rather than distinct subsets. This notion was strengthened by immunophenotyping in situ showing similar frequencies of DC expressing CD2, CD4, and Ox41 in the lamina propria and the epithelial compartment (data not shown). By three-dimensional reconstruction of confocal images we observed that 30–60% of IEDC penetrated the basement membrane (Fig. 1*K*). Taking into account the short half-life of AMDC (<36 h) (8), this finding strongly suggested that there is an extensive continuous trafficking of DC between the lamina propria and the epithelial compartments. Taken together, these findings suggested that lamina propria DC comprised recently recruited small immature "monocyte-like" cells with low

FIGURE 1. Analysis of AMDC under steady-state conditions. Immunofluorescence staining for MHC class II in tracheal epithelium (*A*) and lamina propria (*B*). Images are projections along the *z*-axis ("top view") from stacks of 15 and 6 optical sections, respectively, acquired at 1-μm increments at original magnification of ×600. The exact location of stained cells was readily determined by simultaneous staining with laminin that decorated the surface epithelial basement membrane as shown in *K* (*bottom*). *C*, Flow cytometric analysis of total tracheal digest cells indicating gating for total AMDC (R1) and subregions (R2-R4) based on SSC and MHC class II profiles. *D*, Relative numbers of MHC class II^+ cells within subregions R2-R4. *E* and *F*, Flow cytometric analysis showing FSC and SSC characteristics within subregions R4 and R2-R3, respectively. *G*, Relative number of DC expressing subregion R4 characteristics within the epithelial layer (scrape) and the underlying lamina propria (post scrape) is shown. *H*, Relative number of endocytic activity within subregions R2-R4. *J*, Surface marker expression in R4 subpopulation of total AMDC (R1). *K*, Two-color immunofluorescence staining for MHC class II (red) and laminin (green) in trachea. Projection is shown along the *z*-axis ("top view") of intraepithelial MHC class II^+ cells (*top*). The *yz*-reconstruction of the same image stack (indicated as yellow line in top) visualizing the epithelial basement membrane stained by anti-laminin is shown (*bottom*). Note that many DC penetrate the basement membrane. Data are representative of a series (*A*, *B*, *G*, and *K*) or the mean ± SE from five experiments. Scale bar, 20 μm.

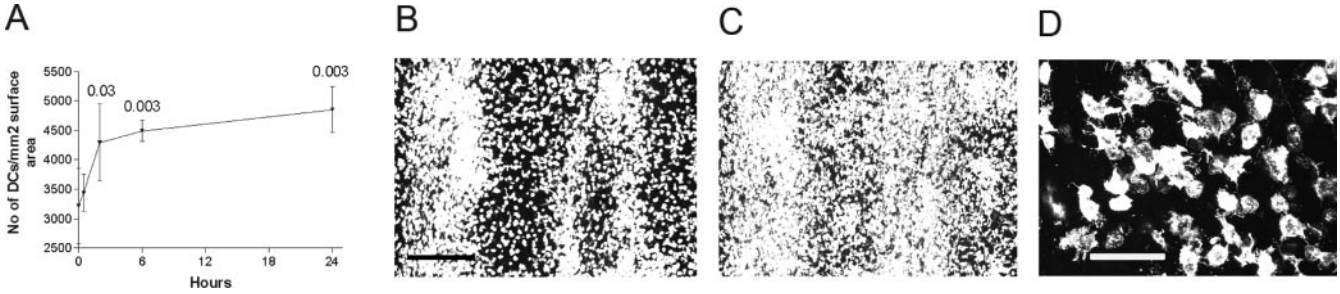

FIGURE 2. In situ analysis of AMDC during bacterial challenge. *A*, Total number of AMDC quantitated by confocal microscopy. *B* and *C*, Representative images of MHC class II$^+$ DC at baseline and 24 h postchallenge, respectively. *D*, Projection from an image stack of 15 optical sections showing lamina propria MHC class II$^+$ DC at 6 h postchallenge. Note many stained cells with long, thin dendrites. Data in *A* are presented as the mean ± SD from at least three separate experiments with at least five animals in each group. Scale bar, 200 μm (*B*) and 40 μm (*D*).

endocytic ability that gradually mature and migrate into the epithelium where they reside as larger DC with high endocytic activity.

Distribution and functional phenotype of AMDC following aerosol challenge with heat-killed M. catarrhalis

In Fig. 2 we analyzed the distribution and functional phenotypes of AMDC after local aerosol challenge with heat-killed *M. catarrhalis* in naive rats. The bacterial challenge resulted in an acute inflammatory response revealed by an intense transient wave of neutrophils that migrated from the mucosa through the epithelial layer and into the airway lumen within 2–6 h (data not shown), as previously described (6). Comparable to our earlier findings (6), we observed a rapid (within 2 h) significant increase ($p < 0.03$) in the total number of AMDC (Fig. 2*A*), which could be readily observed by confocal imaging at low magnification (Fig. 2, *B* and *C*). Concurrently, we observed a transient change in morphology, especially among lamina propria DC. In contrast to the essentially regular/rounded shape characteristic of resting lamina propria DC, at 2 and 6 h postchallenge many lamina propria DC displayed a distinctive dendriform morphology (Fig. 2*D*), which reverted by 24 h to the shape seen in the resting state (data not shown). These in situ changes in AMDC density and morphology were paralleled by an apparent transient change in the overall SSC and MHC class II characteristics of isolated cells assessed by flow cytometry.

At 2 h, the relative number of cells in AMDC subregion R4 was 2-fold increased compared with baseline, whereas the situation was inversely mirrored in the R3 gate (Fig. 3, *A* and *C*). These changes returned to steady-state levels at 12 h postchallenge. These findings corresponded well with the transient change of lamina propria DC morphology (Fig. 2*D*), suggesting that a proportion of lamina propria DC rapidly acquired R4 characteristics in response to the bacterial stimuli. The relative number of R2 cells was significantly increased at 2 and 12 h compatible with an increased recruitment of DC precursors from the circulation (Fig. 3*A*).

The inflammatory response was also accompanied by a minor but significant increase in the number of AMDC expressing the costimulatory molecules CD80 (data not shown) and CD86 within all three subregions (Fig. 3*B*). However, the mean intensity of these markers did not change in any of the regions (Fig. 3*C*). The other functional surface markers examined were relatively stably expressed during the course of challenge, apart from a transient increase of ICAM-1 and Ox41 at 2 h within the R4 subregion (data not shown). The increased number of AMDC expressing MHC class II and costimulatory molecules at 2 h suggested a process of maturation. To gain further evidence for this possibility we sorted AMDC (>95% purity) and examined their capacity to induce T cell proliferation in MLR and measured their endocytic activity. We have previously shown that these two parameters display inverse patterns of change in AMDC in response to cytokine-driven maturation, a marked decline in endocytic function being mirrored by an equally marked increase in MLR activity (5). The ability of DC to stimulate allogeneic T cell proliferation remained equivalent to baseline activity at all time points postchallenge (data not shown). There was no short-term change in endocytic activity within the AMDC population, but a small decrease was observed within the R3 and R4 subpopulations after 12 h (Fig. 3*D*).

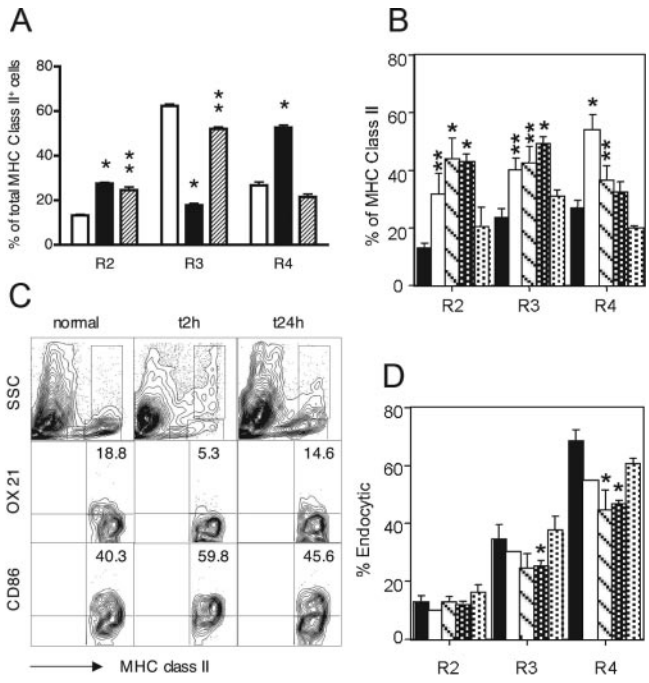

FIGURE 3. Flow cytometric analysis of AMDC during bacterial challenge. *A*, Relative numbers of MHC class II$^+$ DC in subregions R2-R4 at baseline (□), 2 h (■), and 12 h (▨) after challenge. *B*, The percentage of MHC class II$^+$ DC expressing CD86 (after subtraction of control mAb Ox21 surface expression) in subregions R2-R4 at baseline (■), 2 h (□), 12 h (▨), 24 h (white dotted), and 48 h (black dotted) after challenge. *C*, Mean intensity of CD86 expression (*lower*) within the R4 subregion (gating on MHC class II^{high}SSC^{high}, *upper*) at baseline, 2 h, and 24 h. Staining results with isotype- and concentration-matched control mAb Ox21 are shown for comparison (*middle*). *D*, Endocytic activity in subregions R2-R4 at baseline (■), 2 h (□), 12 h (▨), 24 h (white dotted), and 48 h (black dotted) after challenge. Data (*A*, *B*, and *D*) are presented as the mean ± SE from at least three separate experiments with at least five animals in each group. *, $p < 0.01$; **, $p < 0.05$. The representative FACS plots in *C* are from a series of three experiments with at least five animals per group.

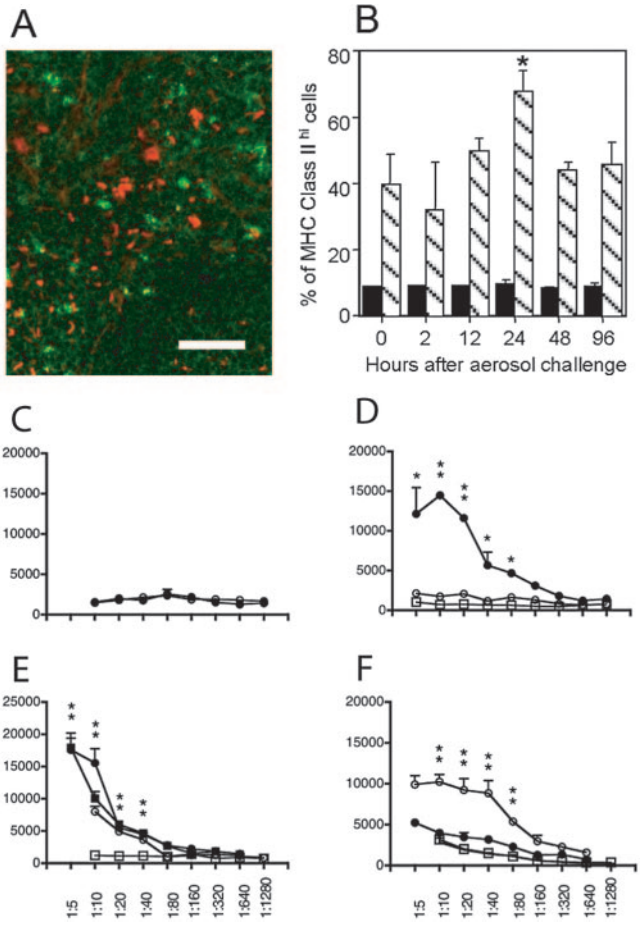

FIGURE 4. Ag transport and presentation by purified mucosal derived DC. *A*, Image of FITC-positive and rhodamine-positive cells in T cell area of cryosection from parathymic LN. FITC and rhodamine dissolved in PBS were simultaneously applied intratracheally and injected i.p., respectively. Parathymic LN were obtained 24 h later. Scale bar, 100 μm. *B*, Relative number of $CD86^+$ cells (▨) among MHC class II^{high} cells of parathymic LN digests before and at various time points after challenge assessed by flow cytometry. Staining results with isotype- and concentration-matched control mAb is shown for comparison (■). *C–F*, DC purified from trachea or parathymic LN of animals challenged with *Moraxella catarrhalis*/OVA or OVA alone were cocultured with $CD4^+$ OVA-specific T cell line for 48 h. T cell proliferation ([^{3}H]DNA synthesis as cpm/culture) is shown as the mean ± SE of triplicates from a representative of at least two independent experiments with at least five animals in each experiment. *C*, OVA presentation of tracheal DC isolated from OVA-naive animals at 2 h (●) and 24 h (○) after *M. catarrhalis*/OVA challenge. *D*, OVA presentation of tracheal DC isolated from OVA-sensitized animals at 2 h (●) and 24 h (○), and OVA-naive animals at 2 h (□) after OVA challenge. *E*, OVA presentation of RLN DC isolated from OVA-naive animals before (□), 0.5 h (■), 2 h (●), and 24 h (○) after *M. catarrhalis*/OVA challenge. *F*, OVA presentation of RLN DC isolated from OVA-sensitized animals at 2 h (●) and 24 h (○), and OVA-naive animals at 24 h (□) after OVA challenge. *, $p < 0.05$; **, $p < 0.005$.

Microbial Ag is rapidly transported by AMDC to RLN

Next we addressed the issue of whether Ag transport from the trachea to the RLN occurs via an active or passive process. We simultaneously administered FITC and TRITC tracers via intratracheal and i.p. routes, respectively, and observed the accumulation of fluorescent positive cells in the parathymic LN, which drain the lymph from both these sites. We reasoned that if the Ags were passively transported to the LN, they would be captured by the same phagocytes within the LN, which would then be visualized as double positive cells. In contrast, if Ags were captured in the periphery and actively transported to the LN, these Ag-bearing cells would appear as positive for a single fluorescent marker. Both under steady-state and inflammatory conditions only single positive cells were observed in tissue sections obtained from parathymic LN (Fig. 4*A* and data not shown). Similar results were obtained when TRITC and FITC were applied intratracheally and i.p., respectively (data not shown). Furthermore, the fluorescent tracers applied intratracheally were virtually exclusively located intracellularly and not found as free Ags in the subcapsular sinus or in the conduits. Flow cytometric analysis of parathymic LN digests showed that fluorescence-labeled DC were $CD86^+$MHC class II^{high} and at 24 h postchallenge the number of cells with this phenotype was significantly increased (Fig. 4*B*). Collectively, these findings are consistent with a general model in which AMDC are able to sample Ags in situ in the airway mucosa and subsequently migrate to the RLN and efficiently present processed peptides to specific T cells.

Although the migratory flux of DC toward RLN increases in both amplitude and speed during acute inflammation (6, 9), there are no published studies available that have addressed the issue of how rapidly postmicrobial challenge pathogen-associated immunogen is delivered to the T memory-generating compartment in RLN. To investigate this question we performed parallel experiments in which OVA was administered with or without aerosolized *M. catarrhalis* to OVA-naive rats and in the latter situation also to OVA-sensitized rats. DC isolated from the trachea and the parathymic LN were subsequently examined for OVA-presenting capacity. In these experiments, DC were sorted to >95% purity from trachea and parathymic LN before and after challenge and then cocultured with OVA-responsive $CD4^+$ T cells for 3 days. Consistent with our MLR data, AMDC isolated from trachea of naive rats challenged with *M. catarrhalis*/OVA aerosol remained unable to stimulate OVA-specific T cells at all time points (Fig. 4*C*), despite the transient up-regulation of costimulator expression on these cells beyond the 2 h time point. This was also the case

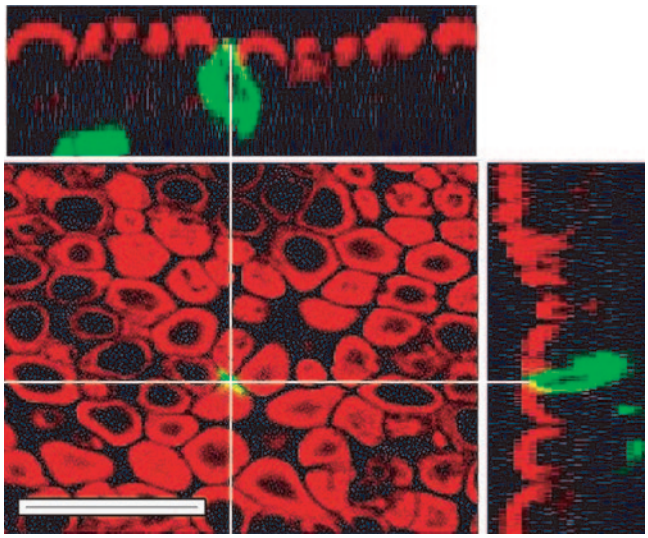

FIGURE 5. In situ three-dimensional reconstruction of IEDC. Immunofluorescence staining for MHC class II (green) and cytokeratin (red) in rat trachea. The *bottom left image* is a projection along the *z*-axis ("top view") from a stack of 15 optical sections acquired in 1-μm increments at original magnification of ×600. The *top* and *right-sided images* are *zx*- and *zy*-reconstructions ("side view") of the same image stack (indicated as yellow lines). These images clearly show that the DC project cellular extension to the apical surface. Scale bar, 20 μm.

with AMDC from OVA-naive rats that were challenged with OVA alone at the 2 h time point (Fig. 4*D*), whereas AMDC isolated from sensitized rats challenged with OVA stimulated OVA-specific T cell proliferation (Fig. 4*D*). A differing pattern of APC activity was observed in the draining parathymic LN. Notably we were able to demonstrate that AMDC harvested from *M. catarrhalis*/OVA-challenged rats capable of presenting processed immunogen to OVA-specific T cells were present in the parathymic LN as early as 30 min after cessation of aerosol exposure (Fig. 4*E*). This Ag-presenting activity was also observed in the parathymic LN at 2 and 24 h. In comparison, OVA-specific APC activity was not observed in the LN of OVA-challenged sensitized rats before the 24 h time point (Fig. 4*F*). Moreover, no APC activity was observed with DC from parathymic LN after aerosolized OVA was administered alone to OVA-naive rats (Fig. 4*F*).

IEDC extend projections into the airway lumen

To visualize the spatial orientation of IEDC in the airway mucosa we performed two-color immunofluorescence of whole mounts combining Abs to MHC class II and cytokeratin. Three-dimensional reconstruction of the image stacks obtained showed that 1–5% of all IEDC both under steady-state conditions and during inflammation projected cellular extensions between the epithelial cells to the apical surface (Fig. 5).

Discussion

In an experimental model of airway allergy we recently showed rapid recruitment of AMDC after OVA-aerosol challenge of OVA-immunized rats (4). In this model, which is replicated as part of the present study, AMDC isolated from the trachea 2 h after OVA challenge efficiently stimulated OVA-specific T cell proliferation, and comparable APC activity was subsequently detected in parathymic LN 24 h postchallenge. Activation of APC function in the airway mucosa in the allergy model was absolutely dependent upon cognate interactions with T memory cells, as no functional OVA-bearing APC were detected within the airway mucosa or parathymic LN of OVA/aerosol-exposed naive animals within the 24 h following exposure.

The present study focused on the effects of a different class of airborne stimuli on naive animals, notably breakdown products of bacteria. We exposed animals to aerosols of heat-killed *M. catarrhalis* admixed with OVA and assessed resulting OVA-specific APC functions in the 24-h period postexposure. We demonstrate that coexposure of rats to OVA and heat-killed *M. catarrhalis* leads to much more rapid appearance of OVA-bearing APC in the parathymic LN (within 30 min of cessation of exposure) relative to that observed with OVA alone. Our results additionally demonstrate that although AMDC rapidly responded to the bacterial stimulus by increasing locally in numbers and to a lesser extent in costimulator expression, similar to that previously observed in the allergy model (4), overall functional maturation within the AMDC population was not completed in situ in the airway mucosa before migration as associated local changes in Ag processing/presentation functions were minimal.

We and others have previously presented indirect evidence that luminal Ags are captured by DC within the airway mucosa and transported to the RLN, rather than passive transportation of free Ag that is subsequently taken up by resident LN APC (4, 10). Studies have demonstrated progressive accumulation of AMDC with strong APC capacity in RLN over time following exposure of the respiratory mucosa to bacterial (6), viral Ags (9), or soluble protein Ags (10, 11). We obtained further confirmation of these observations by simultaneously administering FITC tracer in the trachea and TRITC i.p., or vice versa. Fluorescent microscopy showed that only single positive and not double positive cells were present in tissue sections of parathymic LN without notable extracellular staining, both in the steady state and after challenge. This strongly suggested that the fluorescent tracer had been captured in the periphery and actively transported to the RLN. Collectively these findings are consistent with a general model in which AMDC are able to sample Ags in situ in the airway mucosa and subsequently migrate to the RLN and present processed peptides to specific T cells.

APC functional studies following aerosol exposure to a mixture of OVA and microbial products demonstrated that DC capable of presenting processed Ag to OVA-specific T cells were present in RLN within a short time frame (30 min) postcessation of aerosol exposure. In contrast, we were not able to demonstrate comparable APC activity with tracheal DC at any time point examined, suggesting that the DC population bearing sampled OVA emigrates relatively synchronously from the exposed tracheal mucosa within a relatively short time frame, which is too short to permit full functional maturation before exiting the tissue. A precedent for such efficient "purging" of resident DC from a peripheral challenge site is found in earlier findings (12), demonstrating that intradermal injection of TNF-α rapidly mobilized resident Langerhans cells. *M. catarrhalis* extract stimulates potent TNF-α responses in rat tissue (our unpublished observations) and this mechanism is likely to contribute significantly to the rapid migration kinetics of AMDC observed in this study.

An important unresolved issue, which is central to understanding how immune surveillance of airway tissues operates, concerns the mechanism of penetration of Ags and particulates through the intact epithelium into a milieu in which they can be sampled by AMDC. The central airways relevant to this study are covered by a layer of respiratory epithelial cells that are connected by tight junctions, which form an effective barrier to inhibit paracellular trafficking of most luminal Ags above a molecular mass of ~40 kDa. Assuming that the epithelial barrier was functioning normally in our experimental rats, specific mechanisms for rapid uptake of luminal Ags must be operating constitutively to explain the swift translocation of inhaled Ag to the RLN. Recent data suggest that intestinal DC send up dendrites through the tight junctions without compromising barrier function (13, 14), a phenomenon that allows sampling of luminal Ags through an intact epithelium. Our present findings demonstrate that IEDC in resting and microbial exposed airway mucosa extend projections into the lumen of the airways in a similar fashion, analogous to "snorkeling," and are thus able to capture luminal Ags without disruption of the epithelial barrier. This observation and the finding suggesting that airway IEDC express high endocytic capacity provide a plausible mechanism to explain the extremely rapid transport of inhaled antigenic material to the parathymic LN.

Collectively, the present study demonstrates that AMDC are extremely efficient sentinels in defense against bacterial challenge. They are strategically positioned within the epithelium and capable of sampling luminal Ags through an intact epithelial barrier, and in response to danger signals, which are likely to include TNF-α, they ferry captured luminal Ags to the T cells in the RLN with unexpected rapidity. The kinetics accord well with that reported by Huang et al. (15), which demonstrated that bacterial stimulation induced a much more rapid response in DC compared with fungal or viral exposure. Concomitantly, the accelerated emigration of AMDC in this model is replenished by an increased recruitment of new DC precursors. This danger-driven DC activation in response to bacterial breakdown products is not accompanied by local inflammation, evidenced by minimal T cell activation and the lack of ensuing airway hyperresponsiveness (data not shown). This result

is very different from our earlier allergy model in which the OVA-exposed animals contained OVA-specific T memory cells, and in which inhalation of OVA induced airway mucosal T cell activation and significant airway hyperresponsiveness (2). Future studies in this model should also therefore examine animals preprimed for memory to *M. catarrhalis*.

The possibility that the AMDC population continuously sample the airway luminal surface in the absence of "danger" signals also provides a plausible mechanism for the default response of healthy immunologically naive animals to repeated inhalation of inert soluble protein Ags such as OVA, notably development of a form of immunological tolerance (16, 17). Several studies both in humans and experimental animals have shown that immature DC induce tolerance while only fully activated DC produce immunity (18, 19). These latter findings are consistent with a model in which functionally immature resting AMDC normally sample inhaled Ag passively through intact epithelium, and in the absence of inflammation migrate to RLN and deliver tolerogenic signals to Ag-specific T cells.

It should be noted that stimulus used in this study was restricted to killed bacteria, mimicking the common situation of exposure to airborne bacterial breakdown products that are ubiquitously distributed throughout the indoor and outdoor environments. It will be of interest to extend these studies to live (replicating) organisms, which may provide additional (potentially more potent) signals to the AMDC system, and thus further up-regulate their activity state. Of particular interest will be the events occurring in the airway mucosa of animals preimmunized against the challenge organism.

Disclosures

The authors have no financial conflict of interest.

References

1. Kapsenberg, M. L. 2003. Dendritic-cell control of pathogen-driven T-cell polarization. *Nat. Rev. Immunol.* 3: 984–993.
2. Eisenbarth, S. C., D. A. Piggott, J. W. Huleatt, I. Visintin, C. A. Herrick, and K. Bottomly. 2002. Lipopolysaccharide-enhanced, Toll-like receptor 4-dependent T helper cell type 2 responses to inhaled antigen. *J. Exp. Med.* 196: 1645–1651.
3. Liu, A. H. 2002. Endotoxin exposure in allergy and asthma: reconciling a paradox. *J. Allergy Clin. Immunol.* 109: 379–392.
4. Huh, J. C., D. H. Strickland, F. L. Jahnsen, D. J. Turner, J. A. Thomas, S. Napoli, I. Tobagus, P. A. Stumbles, P. D. Sly, and P. G. Holt. 2003. Bidirectional interactions between antigen-bearing respiratory tract dendritic cells (DCs) and T cells precede the late phase reaction in experimental asthma: DC activation occurs in the airway mucosa but not in the lung parenchyma. *J. Exp. Med.* 198: 19–30.
5. Stumbles, P. A., J. A. Thomas, C. L. Pimm, P. T. Lee, T. J. Venaille, S. Proksch, and P. G. Holt. 1998. Resting respiratory tract dendritic cells preferentially stimulate T helper cell type 2 (Th2) responses and require obligatory cytokine signals for induction of Th1 immunity. *J. Exp. Med.* 188: 2019–2031.
6. McWilliam, A. S., D. Nelson, J. A. Thomas, and P. G. Holt. 1994. Rapid dendritic cell recruitment is a hallmark of the acute inflammatory response at mucosal surfaces. *J. Exp. Med.* 179: 1331–1336.
7. Lambrecht, B. N., B. Salomon, D. Klatzmann, and R. A. Pauwels. 1998. Dendritic cells are required for the development of chronic eosinophilic airway inflammation in response to inhaled antigen in sensitized mice. *J. Immunol.* 160: 4090–4097.
8. Holt, P. G., S. Haining, D. J. Nelson, and J. D. Sedgwick. 1994. Origin and steady-state turnover of class II MHC-bearing dendritic cells in the epithelium of the conducting airways. *J. Immunol.* 153: 256–261.
9. Legge, K. L., and T. J. Braciale. 2003. Accelerated migration of respiratory dendritic cells to the regional lymph nodes is limited to the early phase of pulmonary infection. *Immunity* 18: 265–277.
10. Vermaelen, K. Y., I. Carro-Muino, B. N. Lambrecht, and R. A. Pauwels. 2001. Specific migratory dendritic cells rapidly transport antigen from the airways to the thoracic lymph nodes. *J. Exp. Med.* 193: 51–60.
11. Akbari, O., R. H. DeKruyff, and D. T. Umetsu. 2001. Pulmonary dendritic cells producing IL-10 mediate tolerance induced by respiratory exposure to antigen. *Nat. Immunol.* 2: 725–731.
12. Cumberbatch, M., and I. Kimber. 1995. Tumour necrosis factor-α is required for accumulation of dendritic cells in draining lymph nodes and for optimal contact sensitization. *Immunology* 84: 31–35.
13. Rescigno, M., M. Urbano, B. Valzasina, M. Francolini, G. Rotta, R. Bonasio, F. Granucci, J. P. Kraehenbuhl, and P. Ricciardi-Castagnoli. 2001. Dendritic cells express tight junction proteins and penetrate gut epithelial monolayers to sample bacteria. *Nat. Immunol.* 2: 361–367.
14. Niess, J. H., S. Brand, X. Gu, L. Landsman, S. Jung, B. A. McCormick, J. M. Vyas, M. Boes, H. L. Ploegh, J. G. Fox, et al. 2005. CX3CR1-mediated dendritic cell access to the intestinal lumen and bacterial clearance. *Science* 307: 254–258.
15. Huang, Q., D. Liu, P. Majewski, L. C. Schulte, J. M. Korn, R. A. Young, E. S. Lander, and N. Hacohen. 2001. The plasticity of dendritic cell responses to pathogens and their components. *Science* 294: 870–875.
16. Holt, P. G., J. E. Batty, and K. J. Turner. 1981. Inhibition of specific IgE responses in mice by pre-exposure to inhaled antigen. *Immunology* 42: 409–417.
17. McMenamin, C., and P. G. Holt. 1993. The natural immune response to inhaled soluble protein antigens involves major histocompatibility complex (MHC) class I-restricted $CD8^+$ T cell-mediated but MHC class II-restricted $CD4^+$ T cell-dependent immune deviation resulting in selective suppression of immunoglobulin E production. *J. Exp. Med.* 178: 889–899.
18. Dhodapkar, M. V., R. M. Steinman, J. Krasovsky, C. Munz, and N. Bhardwaj. 2001. Antigen-specific inhibition of effector T cell function in humans after injection of immature dendritic cells. *J. Exp. Med.* 193: 233–238.
19. Steinman, R. M., S. Turley, I. Mellman, and K. Inaba. 2000. The induction of tolerance by dendritic cells that have captured apoptotic cells. *J. Exp. Med.* 191: 411–416.